ACKNOWLEDGMENTS

We thank Michael G. Stabin of the Oak Ridge Associated Universities for assistance in the S-factor validation studies. This work was supported, in part, by the Frank J. Scallon Medical Science Foundation and by NIH grant nos. RO1 CA62444 and UO1 CA58260, and DOE grant no. DE-FG02-86ER-60407.

REFERENCES

1. Snyder WS, Ford MR, Warner GG, Watson EB. "S," absorbed dose per unit cumulated activity for selected radionuclides and organs. *MIRD Pamphlet No. 11*. New York: Society of Nuclear Medicine; 1975.
2. Snyder WS, Ford MR, Warner GG. Estimates of specific absorbed fractions for photon sources uniformly distributed in various organs of a heterogeneous phantom. *MIRD Pamphlet No. 5, Revised*. New York: Society of Nuclear Medicine; 1978.
3. Loevinger R, Budinger TF, Watson EE. *MIRD Primer for Absorbed Dose Calculations*. New York: Society of Nuclear Medicine; 1991.
4. Leichner PK, Kwok CS. Tumor dosimetry in radioimmunotherapy: methods of calculation for beta particles. *Med Phys* 1993;20:529–534.
5. Meredith RF, Johnson TK, Plott G, et al. Dosimetry of solid tumors. *Med Phys* 1993;20:583–592.
6. Stabin MG. MIRDOSE—the personal computer software for internal dose assessment in nuclear medicine. *J Nucl Med* 1996;37:538–546.
7. Johnson TK. MABDOS: a generalized program for internal radionuclide dosimetry. *Comput Methods Programs Biomed* 1988;27:159–167.
8. Sgouros G, Chiu S, Pentlow KS, et al. Three-dimensional dosimetry for radioimmunotherapy treatment planning. *J Nucl Med* 1993;34:1595–1601.
9. Erdi AK, Wessels BW, DeJager R, et al. Tumor activity confirmation and isodose curve display for patients receiving iodine-131-labeled 16.88 human monoclonal antibody. *Cancer* 1994;73:(suppl):932–944.
10. Sgouros G, Barest G, Thekkumthala J, et al. Treatment planning for internal radionuclide therapy: three-dimensional dosimetry for nonuniformly distributed radionuclides. *J Nucl Med* 1990;31:1884–1891.
11. Giap HB, Macey DJ, Bayouth JE, Boyer AL. Validation of a dose-point kernel convolution technique for internal dosimetry. *Phys Med Biol* 1995;40:365–381.
12. Giap HB, Macey DJ, Podoloff DA. Development of a SPECT-based three-dimensional treatment planning system for radioimmunotherapy. *J Nucl Med* 1995;36:1885–1894.
13. Tagesson M, Ljungberg M, Strand SE. Transformation of activity distribution in quantitative SPECT to absorbed dose distribution in a radionuclide treatment planning system [Abstract]. *J Nucl Med* 1994;123P.
14. Furhang EE, Chui CS, Sgouros G. A Monte Carlo approach to patient-specific dosimetry. *Med Phys* 1996;23:1523–1529.
15. van Dieren EB, van Lingen A, Roos JC, Teule GJJ. Validation of the distance histogram technique for three-dimensional and two-dimensional dosimetric calculations. *Appl Rad Isot* 1992;43:1211–1221.
16. Kolbert KS, Sgouros G, Scott AM, et al. Dose-volume histogram representation of patient dose distribution in three-dimensional internal dosimetry [Abstract]. *J Nucl Med* 1994;35:123P.
17. Kolbert KS, Sgouros G, Graham MC, Larson SM. Display and analysis of multimodality registered images [Abstract]. *J Nucl Med* 1995;36:125P.
18. Rew R, Davis G, Emmerson S. *NetCDF user's guide. An interface for data access*, version 2.3. Boulder, CO: Unidata Program Center, University Corporation for Atmospheric Research; 1993.
19. Furhang EE, Sgouros G, Chui CS. Radionuclide photon dose kernels for internal emitter dosimetry. *Med Phys* 1996;23:759–765.
20. Prestwich WV, Nunes J, Kwok CS. Beta dose point kernels for radionuclides of potential use in radioimmunotherapy. *J Nucl Med* 1989;30:1036–1046.
21. Simpkin DJ, Mackie TR. EGS4 monte carlo determination of the beta dose kernel in water. *Med Phys* 1990;17:179–186.
22. Leichner PK. A unified approach to photon and beta particle dosimetry. *J Nucl Med* 1994;35:1721–1729.
23. Cristy M, Eckerman KF. In: Specific absorbed fractions of energy at various ages from internal photon sources. *ORNL/TM-8381/V1*. Oak Ridge, TN: ORNL 1987.
24. Duda RO, Hart PE. *Pattern recognition and scene analysis*. New York: Wiley; 1973.
25. Caron PC, Jurcic JG, Scott AM, et al. A phase I B trial of humanized monoclonal antibody M195 (anti-CD33) in myeloid leukemia: specific targeting without immunogenicity. *Blood* 1994;83:1760–1768.
26. Pelizzari CA, Chen GTY. Registration of multiple diagnostic imaging scans using surface fitting. In: *Proceedings of the Ninth International Conference on Use of Computers in Radiation Therapy*. 1987:437–440.
27. Sgouros G, Jureidini IM, Scott AM, Graham MC, Larson SM, Scheinberg DA. Bone marrow dosimetry: regional variability of marrow-localizing antibody. *J Nucl Med* 1996;37:695–698.
28. Divgi CR, Scott AM, Dantis L, et al. Phase I radioimmunotherapy trial with iodine-131-CC49 in metastatic colon carcinoma. *J Nucl Med* 1995;36:586–592.
29. Scott AM, Macapinlac H, Zhang JJ, et al. Clinical applications of fusion imaging in oncology. *Nucl Med Biol* 1994;21:775–784.

Patient-Specific Dosimetry Using Quantitative SPECT Imaging and Three-Dimensional Discrete Fourier Transform Convolution

Gamal Akabani, William G. Hawkins, Miriam B. Eckblade and Peter K. Leichner
Department of Radiation Oncology, University of Nebraska Medical Center, Omaha, Nebraska

The objective of this study was to develop a three-dimensional discrete Fourier transform (3D-DFT) convolution method to perform the dosimetry for ^{131}I-labeled antibodies in soft tissues. **Methods:** Mathematical and physical phantoms were used to compare 3D-DFT with Monte Carlo transport (MCT) calculations based on the EGS4 code. The mathematical and physical phantoms consisted of a sphere and a cylinder, respectively, containing uniform and nonuniform activity distributions. Quantitative SPECT reconstruction was carried out using the circular harmonic transform (CHT) algorithm. **Results:** The radial dose profile obtained from MCT calculations and the 3D-DFT convolution method for the mathematical phantom were in close agreement. The root mean square error (RMSE) for the two methods was <0.1%, with a maximum difference <21%. Results obtained for the physical phantom gave a RMSE <0.1% and a maximum difference of <13%; isodose contours were in good agreement. SPECT data for two patients who had undergone ^{131}I radioimmunotherapy (RIT) were used to compare absorbed-dose rates and isodose rate contours with the two methods of calculation. This yielded a RMSE <0.02% and a maximum difference of <13%. **Conclusion:** Our results showed that the 3D-DFT convolution method compared well with MCT calculations. The 3D-DFT approach is computationally much more efficient and, hence, the method of choice. This method is patient-specific and applicable to the dosimetry of soft-tissue tumors and normal organs. It can be implemented on personal computers.

Key Words: Monte Carlo calculations; SPECT; dosimetry; fast Fourier transform

J Nucl Med 1997; 38:308–314

The development of patient-specific dosimetry for administered radionuclides and radiolabeled compounds is essential for a better understanding of tumor response and normal-tissue toxicity. This is particularly relevant in clinical trials in cancer therapy with large administered activities and potentially high radiation-absorbed doses in tumors and normal tissues. As discussed previously, in clinical trials, the absorbed dose is usually calculated rather than measured, and calculations are

Received Nov. 8, 1995; revision accepted Apr. 5, 1996.

For correspondence or reprints contact: Gamal Akabani, PhD, Department of Radiation Oncology, University of Nebraska Medical Center, Box 981045, 600 South 42nd St., Omaha, NE 68198-1045.

usually based on imaging procedures (*1*). Therefore, a necessary first step in nuclear medicine dosimetry was the development of algorithms and computer software for activity quantitation in tumors and normal tissues as a function of time.

After the spatial and temporal distribution of radioactivity has been determined for a patient, patient-specific radiation-absorbed dose calculations can be determined. In principle, Monte Carlo calculations of the transport of radiation could be used for patient-specific dosimetry. In practice, such calculations are computationally very intensive and time-consuming (*2,3*). An alternative method is to use point-dose kernels which permit assessment of absorbed dose rate and dose in a more efficient manner (*4–7*). However, point kernels only apply to homogeneous tissues.

In this report, we generalize previous work on a unified approach to photon and beta-particle dosimetry (*6*) and introduce a point-source kernel for ^{131}I which includes not only photons and beta particles but also monoenergetic electrons. We show that a three-dimensional convolution method using a discrete Fourier transform (3D-DFT) permits efficient computations of absorbed-dose rates for ^{131}I. We chose this radionuclide for the present study because it is widely used in diagnostic and therapeutic nuclear medicine and because its spectrum is sufficiently complex to test this approach to dosimetry. We demonstrate explicitly in mathematical and physical phantom studies and in two patient studies that the 3D-DFT method is as accurate as Monte Carlo transport (MCT) calculations. This means that in conjunction with quantitative SPECT, based on the circular harmonic transform (CHT) algorithm (*8–11*), we have developed and clinically implemented a system for patient-specific soft-tissue dosimetry.

In the three-dimensional absorbed-dose calculations described in this report, every voxel in a SPECT matrix represents both a source and a target volume. Calculations therefore yield distributions of absorbed-dose rates and dose-rate gradients that are characterized by isodose rate contours and dose-rate volume histograms. An important feature of the output of absorbed-dose calculations in our approach to patient-specific dosimetry is the superposition of isodose rate contours on SPECT images. Additionally, minimum, maximum and mean values of absorbed-dose rates are computed for each volume of interest (VOI). VOIs are user-defined manually or by using an activity threshold level. These features provide a complete description of absorbed-dose rates at each time point. The absorbed dose is obtained by integrating over several time points, which include at least two SPECT studies and several whole-body images acquired over a period of days.

The results of this work differ from previous investigations (*2,5,7*) in several aspects. The 3D-DFT absorbed-dose calculations are shown to yield the same results as Monte Carlo calculations. The 3D-DFT method is computationally more efficient. This means that three-dimensional absorbed-dose calculations can be carried out on computers in nuclear medicine departments and on currently available personal computers. Furthermore, all calculations are based on three-dimensional SPECT matrices and do not require additional input from other imaging modalities, although these may be helpful in identifying VOIs. Finally, a more complete description of absorbed-dose rates and dose is provided than was done previously.

MATERIALS AND METHODS

Monte Carlo transport calculations were determined using the EGS4 code (*12,13*). Electron and photon transport calculations were determined with a cut-off energy of 10 keV. Patient SPECT data were acquired with a dual-headed gamma camera system. Tomographic reconstruction was carried out using the circular harmonic transform (CHT) algorithm (*8*) and transverse SPECT slices were reconstructed in 128 × 128 matrices. The basic element of the SPECT matrix was a cubic voxel with a side dimension of 0.467 cm. Calculations were determined for ^{131}I, a widely used radionuclide in diagnostic and therapeutic nuclear medicine.

TABLE 1
Discrete Absorbed Dose Kernel Representation in Water for Iodine-131 in an Infinite Lattice Based on Voxel Index and Radial Distance

Index ($i^2 + j^2 + k^2$)	Radial distance (cm)	No. of voxels	Absorbed dose (Gy/Bq s)
0	0.00000	1	2.733×10^{-10}
1	0.46693	6	6.329×10^{-12}
2	0.66033	12	5.911×10^{-13}
3	0.80874	8	2.706×10^{-13}
4	0.93385	6	1.940×10^{-13}
5	1.04410	24	1.524×10^{-13}
6	1.14370	24	1.260×10^{-13}
8	1.32070	12	9.765×10^{-14}

Radionuclide Kernel

A single kernel containing all types of emitted radiations was generated for use in the 3D-DFT convolution method. The basic convolution kernel was calculated by MCT. Photon and electron transport were performed in a lattice where the source region was located at the voxel of origin (with coordinate indexes i = 0, j = 0, k = 0) containing a uniform activity distribution. The decay scheme and beta spectrum for ^{131}I were obtained from the National Nuclear Data Center (NNDC, Brookhaven Natl. Lab., Upton, NY) and by using the Program RADLST (*14*). MCT calculations were then performed and energy deposition was computed for every voxel of the lattice. The number of histories transported was 10 million, requiring an elapsed running time of approximately 10 hr on a personal computer. The cubic voxel dimensions were the same as in the SPECT matrix. This kernel representation was not continuous but rather discrete, based on the absorbed dose to every individual voxel of the lattice. Table 1 presents the initial elements of the discrete kernel for ^{131}I based on the voxel index, defined as $m^2 = i^2 + j^2 + k^2$, and radial distance. Figure 1 illustrates the absorbed dose kernel as a function of radial distance. Statistical

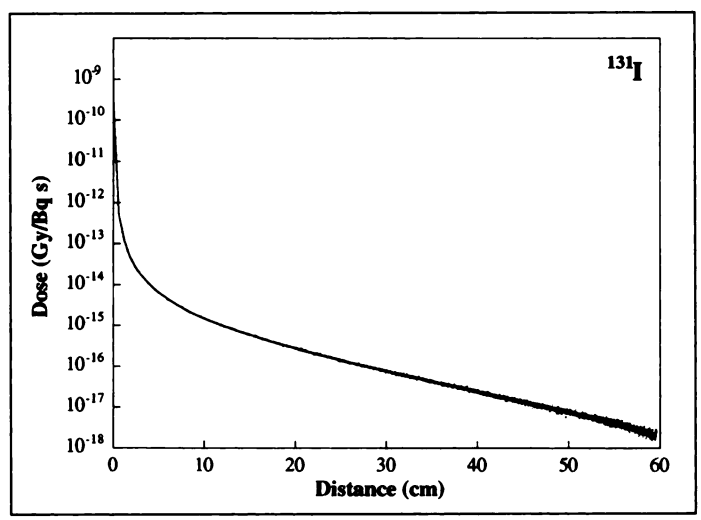

FIGURE 1. Dose kernel for ^{131}I based on a cubic voxel of 0.467 cm side. This kernel contains both electron and photon components and was calculated using the EGS4 MCT code. The material used was water with a density of 1.00 g/cm^3.

errors were calculated based on energy deposition for voxels having the same index, m^2. Therefore, these statistical errors were proportional to the radial distance from the center of the lattice and inversely proportional to the number of voxels with the same index. The maximum standard deviation calculated was 450% for the voxel with index $m^2 = 16293$ at a distance of 59.6 cm. This kernel representation takes advantage of the symmetry of a cubic lattice, thus reducing the amount of computer memory used to store the kernel. A 128 × 128 × 128 matrix required 8.4 MB of memory; but when symmetry was applied and the kernel was transformed into an ASCII format, the file size was reduced to approximately 300 kB. This ASCII file was later used to generate the 128 × 128 × 128 matrix containing the three-dimensional dose kernel required during the 3D-DFT convolution process. This process was performed by calculating the index value m^2 of a given voxel and, thus, the corresponding kernel value for every voxel of the matrix. The origin of the indices (i, j, k) was located at the center of the matrix. This kernel representation depends on the matrix voxel size; but it is irrespective of the radiations being emitted and could be applied to any other radionuclide decay scheme.

Monte Carlo Source Sampling

To implement MCT calculations, it was necessary to perform source sampling based on the activity distribution in SPECT images. A triple-rejection technique based on conditional activity distributions was used to sample the indices i, j, k over the three-dimensional matrix. This was done by collapsing the activity distribution over the z-axis and carrying out an initial rejection technique. After k was evaluated, a second pass through the rejection technique was used to assess j by collapsing the corresponding z plane over the y-axis, and finally, i was evaluated based on the evaluated k and j indices. These probability distributions were expressed as

$$h^z(k) = \sum_i \sum_j A(i, j, k), \qquad \text{Eq. 1}$$

$$h^y(j; k) = \sum_i A(i, j; k), \qquad \text{Eq. 2}$$

and

$$h^x(i; j, k) = A(i; j, k), \qquad \text{Eq. 3}$$

where $h^z(k)$ was the probability distribution on the z-axis; $h^y(j; k)$ was the conditional probability distribution on the y-axis given k, and $h^x(i; j, k)$ was the conditional probability distribution on the x-axis given j and k. Consider a matrix of size M × M × N, where M is the slice matrix dimension and N the number of reconstructed SPECT slices. There will be one single probability function for the z-axis and the corresponding h^z_{max}, N conditional probability distributions for the y-axis and their corresponding $h^y_{max}(k)$, and M × N conditional probability distributions for the x-axis and their corresponding $h^x_{max}(j, k)$. Once the voxel indices (i, j, k) were calculated, the coordinates (x, y, z) were sampled based on a uniform activity distribution in a given voxel. This was expressed as follows:

$$\begin{aligned} x &= i\Delta + (\text{ran} - 0.5)\Delta \\ y &= j\Delta + (\text{ran} - 0.5)\Delta \\ z &= k\Delta + (\text{ran} - 0.5)\Delta, \end{aligned} \qquad \text{Eq. 4}$$

where Δ was the cubic voxel side dimension and ran is a random number. This method was extremely efficient in comparison to a simple rejection technique that samples simultaneously the x-, y- and z-axis; however, it required twice the computer memory for source sampling. Photon and electron MCT calculations were determined to assess the energy deposition patterns and absorbed dose rates based on a given activity distribution. To obtain reliable results from MCT calculations, a minimum of 4 million histories was required to carry out a comparative study.

CHT Algorithm

The CHT SPECT algorithm consists of two main elements: (a) an attenuation correction based on uniform attenuation within a convex body and (b) a two-dimensional Wiener prefilter based on measurements of the point spread function of the SPECT imaging system. The attenuation correction consists of a fast contouring algorithm that generates a convex body contour directly from the projection data, and a correction for uniform attenuation based on two-dimensional Fourier inversion (*8,15*). This method has significantly higher signal-to-noise ratios than exponential backprojection and has been shown to be a member of a class of algorithms for the inversion of the exponential radon transform (*16*) that are characterized by a single parameter with physical significance. This parameter represents the proportion of "near field" and "far field" signals, which are stochastically nonredundant but correlated and are utilized in the reconstruction. The two-dimensional Wiener prefilter of the planar projection data is a stationary filter, and is the sum of a gaussian function representing collimator resolution and a function representing scatter. The characterization of collimator FWHM and scatter fraction is determined by a series of point source measurements in air and in Plexiglass as the scattering medium. The variance of the two-dimensional Fourier transform, which is used as an estimate of the noise power spectrum in the Wiener filter, is modified by the premultiply step in the attenuation correction (*17*). This protocol has been evaluated in human and animal studies (*10,11*).

3D-DFT Convolution

The absorbed dose rate to a point in space from a given activity distribution can be expressed in terms of the convolution integral

$$D(r_0) = \int_{Vol} k(r - r_0)A(r)dr^3, \qquad \text{Eq. 5}$$

or

$$D(r_0) = k(r_0) * A(r_0), \qquad \text{Eq. 6}$$

where $D(r_0)$ gives the dose rate at point r_0, A(r) is the spatial activity distribution, and k(r) is the radiation dose kernel for all radiative components of a radionuclide. The Fourier transform (FT) of the convolution in Equation 6 is:

$$FT\{D(r)\} = FT\{k(r)\}FT\{A(r)\}. \qquad \text{Eq. 7}$$

In other words, the convolution of two functions in the spatial domain corresponds to the product of the Fourier transform of the two signals in the frequency domain. However, the SPECT data were represented in a discrete three-dimensional matrix rather than a continuous function. Thus, a discrete Fourier transform (DFT) was used as a fundamental operation to assess absorbed dose and dose-rate distributions in discrete space (*18*). In discrete space, the convolution of two discrete functions, k(n) and A(n) is defined by:

$$D(n) = \sum_{m=-\infty}^{m=\infty} k(n - m)A(n) \qquad \text{Eq. 8}$$

and this can be denoted again as

$$D(n) = k(n) * A(n). \qquad \text{Eq. 9}$$

When applying the DFT, this becomes:

$$DFT\{D(n)\} = DFT\{k(n)\}DFT\{A(n)\}. \qquad \text{Eq. 10}$$

The DFT converts the convolution into multiplication. This property was used to reduce the computations needed for convolution by using the following equation:

$$D(n) = IDFT\{DFT\{k(n)\}DFT\{A(n)\}\}, \qquad \text{Eq. 11}$$

where IDFT represents the inverse discrete Fourier transform.

RESULTS

Comparison of MCT and 3D-DFT Convolution for Mathematical Phantoms

To assess the accuracy of the 3D-DFT convolution method, three tests were performed for a sphere containing different activity distributions where the radial dose profile was calculated from the center of the sphere. The sphere was set up at the center of a 128 × 128 × 128 matrix containing different activity distributions of ^{131}I. The regions inside and outside the sphere were assumed to be made up of water with a density of 1.00 g/cm^3. Monte Carlo sampling was based on the triple conditional rejection technique described above. The sphere setup was based on the indices i, j, k where

$$(i - 64)^2 + (j - 64)^2 + (k - 64)^2 \leq 16^2. \qquad \text{Eq. 12}$$

The root mean square error (RMSE) of each dataset was calculated to assess the overall difference in the results obtained between the 3D-DFT convolution method and MCT. The root mean square error was calculated as expressed by:

$$RMSE = \frac{\sqrt{\sum_{i,j,k} (\alpha_{i,j,k} - \beta_{i,j,k})^2}}{\sum_{i,j,k} \beta_{i,j,k}}, \qquad \text{Eq. 13}$$

where $\alpha_{i,j,k}$ and $\beta_{i,j,k}$ are the results obtained from MCT and the 3D-DFT convolution method, respectively. Moreover, the maximum difference was calculated as expressed by:

$$\partial = \max\left(\frac{|\alpha_{i,j,k} - \beta_{i,j,k}|}{\beta_{i,j,k}}\right). \qquad \text{Eq. 14}$$

The first test consisted of a uniform distribution of ^{131}I in a sphere. CT was performed for 4 million histories and results were normalized to absorbed dose per unit transformation (Gy/Bq s). Figure 2A shows the comparison of the results as calculated from MCT and the 3D-DFT where the absorbed dose profile is expressed as a function of radial distance (cm) from the center of the sphere. The agreement between MCT and the 3D-DFT convolution reflects the precision of the 3D-DFT convolution for regions inside and outside the sphere. The differences between the methods are due to the stochastic nature of MCT and computational approximations associated with the 3D-DFT convolution method. The MCT standard deviation for every voxel in the matrix was calculated. For regions with high activity content the standard deviation was between 10% to 150%; however, for regions with no activity content the standard deviation varied from 150% to 520%. The computer time required to run MCT was approximately 18 hr. The RMSE for the whole dataset was 0.04%, and the maximum difference, ∂, was 21%.

The second test consisted of two concentric spheres containing a uniform distribution of ^{131}I. The concentration ratio between the inner and outer spheres was 10:1. MCT calculations were performed for 4 million histories. Figure 2B illustrates the dose profile for this geometrical arrangement. The radial dose profile for both MCT and 3D-DFT convolution method were in very close agreement. The RMSE for the whole dataset was 0.04%, and the maximum difference, ∂, was 10%.

The third test consisted of a sphere containing an activity distribution inversely proportional to the radius of the sphere. In this case, MCT was determined for 40 million histories, and Figure 2C illustrates the dose profile for both MCT and 3D-DFT. Again, the differences between MCT and 3D-DFT were due to the stochastic behavior of MCT. The RMSE for the whole dataset was 0.02%, and the maximum difference, ∂, was 1.5%.

TABLE 2
Measured and Calculated Activity Concentrations in a Nonuniform Phantom

Region	Measured activity (μCi/ml)	Calculated activity (μCi/ml)	Difference (%)
Cold	0.00	0.15	—
Background	1.28	1.27	−0.78
Hot	3.55	3.14	−11.55

Calculated activities were based on reconstructions using the CHT algorithm.

Comparison of MCT and 3D-DFT Convolution for Physical Phantom Studies

Phantom studies were performed to assess the applicability of the 3D-DFT convolution method with our current methods for quantitative SPECT imaging. A cylindrical phantom with an inside diameter of 21.5 cm and an inside height of 18.5 cm was filled with water. A nonuniform phantom study was performed to assess the applicability of the 3D-DFT convolution method

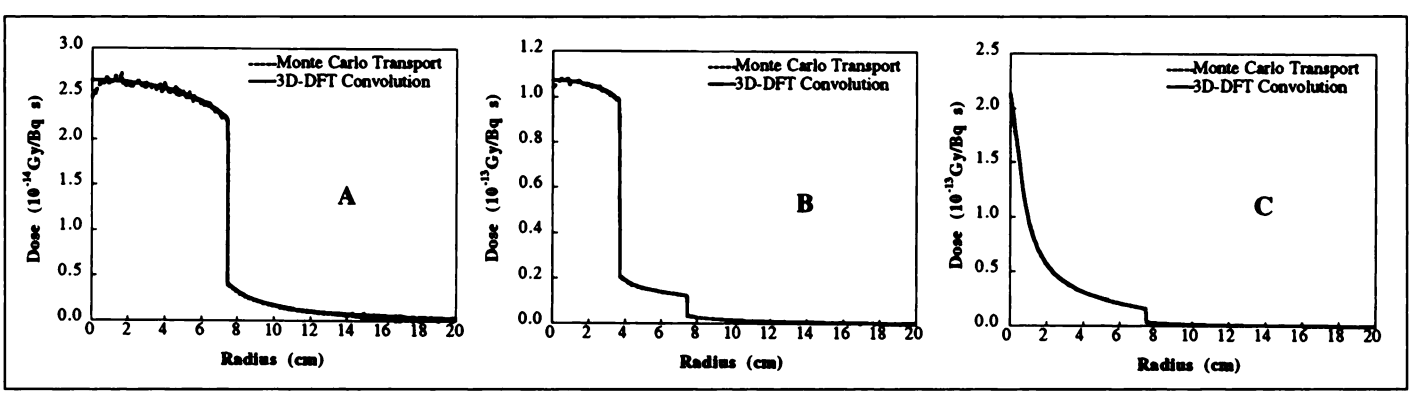

FIGURE 2. Radial dose profiles as calculated with MCT and the 3D-DFT convolution method for different activity distributions of ^{131}I in a sphere of 7.47 cm. (A) Uniform activity distribution. (B) Two concentric regions with an activity concentration of 1:1. (C) Activity concentration proportional to $(m^2 + 1)^{-1/2}$, where $m^2 = i^2 + j^2 + k^2$.

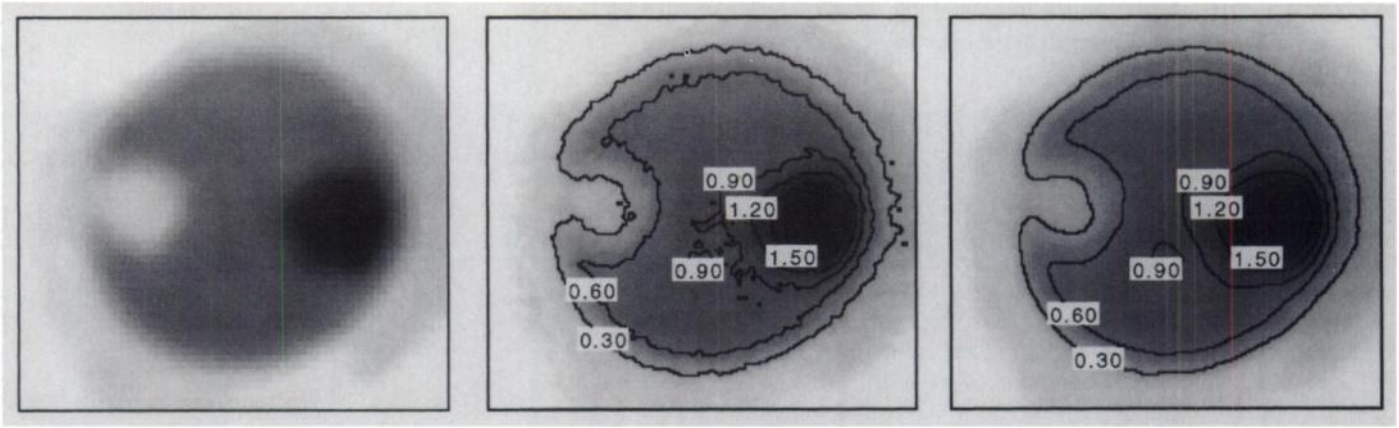

FIGURE 3. Comparison of MCT and 3D-DFT convolution isodose-rate (cGy/hr) contours of a SPECT cylindrical phantom for ^{131}I containing a cold background and hot region.

for nonuniform regions. The phantom consisted of hot, cold and background activity regions. Two inner cylinders were used to represent the hot and cold regions. One inner cylinder was filled with plain water simulating a cold region. The inner cylinders each had a volume of 570 ml and an inside diameter of 7.26 cm. SPECT reconstruction was performed using the CHT algorithm. Table 2 shows a comparison between the measured and calculated activity concentrations in the cold, background and hot regions. Monte Carlo transport calculations were determined for 40 million histories using the activity concentrations calculated by the CHT algorithm. Voxels outside the phantom contour with nonzero activity levels were discarded. Figure 3 illustrates a comparison of isodose rate contours results obtained using MCT and the 3D-DFT convolution method. The RMSE for the whole dataset was 0.01%, and the maximum difference, ∂, was 12.4%.

In many instances, the SPECT data do not contain all possible activity distributions over the body; thus, absorbed dose rates to regions that are close to the initial and last SPECT slice may be underestimated because activity regions that are located above the first and below the last reconstructed SPECT slices are not taken into account. To quantitatively assess this possible underestimation, a cylindrical phantom containing a uniform activity distribution of ^{131}I was used. Twenty-five slices were reconstructed and absorbed dose rates were calculated using the 3D-DFT convolution method. The percentage differences in absorbed dose rates were calculated based on one, two, four and eight missing slices, where these slices have the same activity concentration and were located prior to slice 1. Figure 4 illustrates the profile of the difference of the mean absorbed dose rate as a function of the slice number based on the number of missing slices. This difference is proportional to the number of missing slices. As expected, however, this difference becomes smaller for those regions that are farther away from the boundary. This dose rate underestimation needs to be avoided if precise absorbed dose rate estimates are to be obtained. Thus, when performing SPECT reconstruction, regions of high activity content need to be fully reconstructed and contain all VOIs.

Patient-Specific Dosimetry Using Quantitative SPECT Imaging

To study the feasibility of using the 3D-DFT convolution method in clinical trials, SPECT data from two patient who had undergone ^{131}I RIT were used. Patient-specific dosimetry was determined using a SPECT reconstruction matrix of 128 × 128 by N slices. Because no image registration was used to delimit the boundaries of different organs and regions of the body, all regions were assumed to be made of a single tissue equivalent material with density of 1.04 g/cm^3(*19,20*). A convolution kernel for ^{131}I was then calculated for this material type and density. Absorbed dose rates based on the 3D-DFT convolution method were calculated using calculated using Equation 11. Similarly, MCT calculations were determined for 40 million histories to assess the dose rate profile. A comparison of the results obtained with MCT calculations and the 3D-DFT convolution method for both SPECT datasets delivered an overall RMSE of less than 0.02%, and a maximum difference, ∂, of less than 13%. Figure 5 shows the isodose contours obtained using both methods for a transverse slice from each SPECT dataset. With this method, it was possible to assess dose-rate gradients for regions and organs of the body and, furthermore, given a VOI, it was possible to assess a dose-rate volume histogram. For example, the liver was selected as a VOI in which all regions were determined in all reconstructed slices. Consequently, it was possible to perform an analysis of the VOI based on dose-rate volume histograms and calculate the maximum, minimum, and mean dose rates and their corresponding standard deviation (Fig. 6).

DISCUSSION

The comparison of results of MCT calculations and 3D-DFT convolution for both mathematical and physical phantoms shows that the latter method is a precise tool to determine

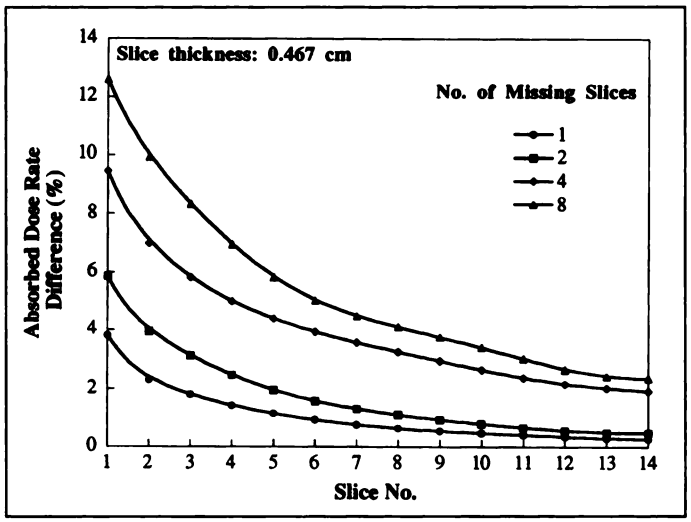

FIGURE 4. Percentage difference of absorbed dose rate as a function of slice number based on the number of missing slices for a cylindrical phantom with a uniform distribution of ^{131}I.

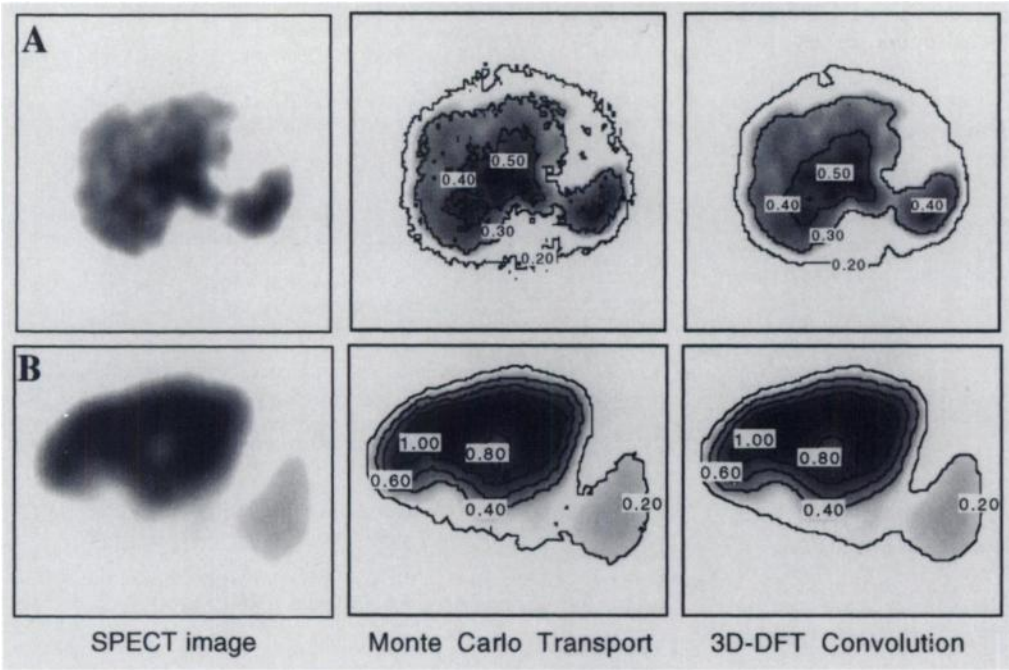

FIGURE 5. Comparison of MCT and 3D-DFT convolution isodose-rate contours (cGy/hr). SPECT slices of the liver and spleen of two patients who had undergone ^{131}I RIT.

absorbed dose and dose rate profiles. Therefore, the 3D-DFT convolution method can be used on a patient-specific basis to determine radiation dosimetry of tumors, organs and user-defined VOIs. In contrast to the current MIRD methodology (*21*), this method allows us to generate isodose rate contours, dose-rate gradients, dose-rate volume histograms (both differential and cumulative) and perform statistical analysis, rather than simply assess average absorbed doses or dose rates based on assumed uniform activity distributions over predefined organs and regions. Consequently, this dosimetric method may help assess the effectiveness of a specific radionuclide therapy on a patient-specific basis, rather than simply assess average absorbed doses to gross anatomical regions.

However, it is important to address the limitation of this convolution method. First, the 3D-DFT convolution method is only valid for those regions of the body with a uniform density. Therefore, the results will underestimate or overestimate absorbed doses to the lungs, bone and interface regions. However, a study by Sauer (*22*) indicates that it is possible to implement a convolution and superposition method to assess absorbed dose rates for nonuniform regions and interfaces, as is the case for bone and lung soft tissues. Furthermore, to outline regions and organs of different material type and density, it will be important to use CT-SPECT or MRI-SPECT image registration techniques.

The second limitation is based on the number of reconstructed SPECT slices that describe the spatial activity distribution over the body. As shown in this study, an underestimation of the absorbed dose rate to regions and organs of the body may occur if activity regions that are beyond the first and last reconstructed slice are ignored. For ^{131}I, this dose rate underestimation can be up to 20% for regions close to the boundaries of reconstruction. However, this limitation can be avoided as long as the VOIs are located well within the first and last SPECT-reconstructed slices.

CONCLUSION

The 3D-DFT convolution method presented here was used to calculate absorbed doses and dose rates for a given activity distribution in a computationally efficient manner. The com-

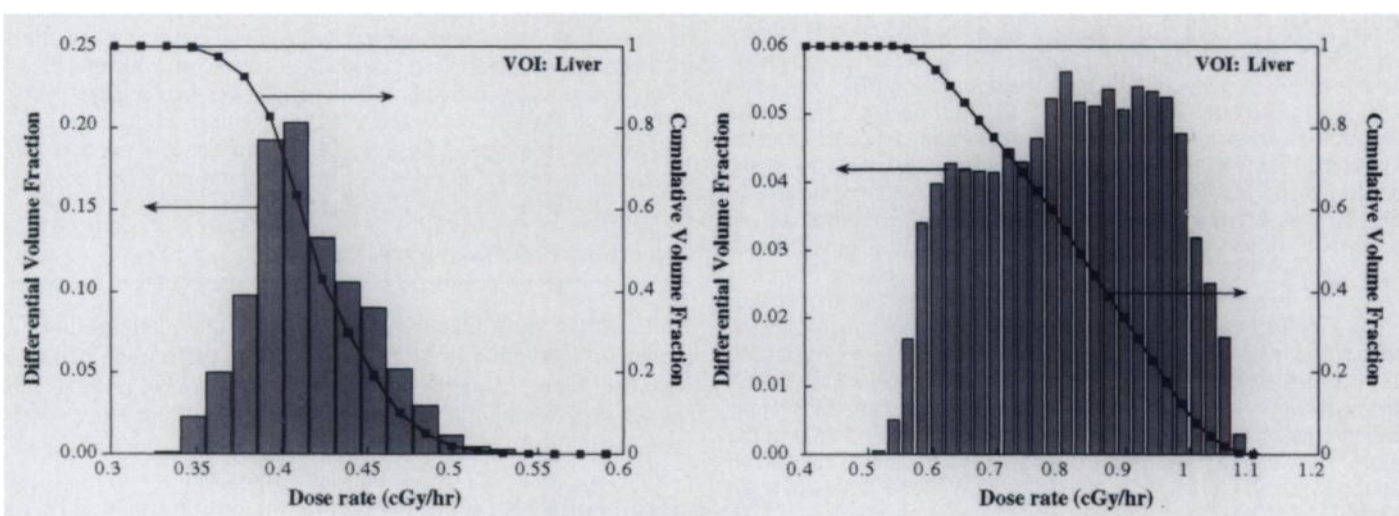

FIGURE 6. Examples of differential and cumulative dose-rate volume histograms for the liver based on quantitative SPECT imaging and 3D-DFT convolution for two patients who had undergone ^{131}I RIT. Mean absorbed dose rate and standard deviation were: (A) 0.42 and 0.06 (cGy/hr) and (B) 0.81 and 0.14 (cGy/hr), respectively.

parison of results of MCT calculations and 3D-DFT convolution shows that the latter method is a precise tool for determining absorbed dose and dose-rate profiles for any given spatial activity distribution. Thus, the 3D-DFT convolution method can be used on a patient-specific basis to determine the dosimetry of tumors, organs and user-defined VOIs.

ACKNOWLEDGMENTS

This work was supported in part by Department of Energy grant DE-FG02-91ER61195 and National Cancer Institute grant U01 CA58272-03.

REFERENCES

1. Leichner PK, Koral KF, Jaszczak RJ, Green AJ, Chen GTY, Roeske JC. An overview of imaging techniques and physical aspects of treatment planning in radioimmunotherapy. *Med Phys* 1993;20:569–577.
2. Johnson TK. MABDOS: A generalized program for internal radionuclide dosimetry. *Comput Meth Progr Biomed* 1988;27:159–167.
3. Meredith RF, Johnson TK, Plott G, et al. Dosimetry of solid tumors. *Med Phys* 1993;20:583–592.
4. Berger MJ. Beta-ray dosimetry calculations with the use of point kernels. In: Cloutier RJ, Edwards CL, Snyder WS, eds. *Medical radionuclides: radiation dose and effects.* Oak Ridge, TN: AEC Symposium Series No. 20, CONF 691212; 1970;36–42.
5. Sgouros G, Barest G, Tekumthala J, et al. Treatment planning for internal radionuclide therapy: three-dimensional dosimetry for nonuniformly distributed radionuclides. *J Nucl Med* 1990;31:1884–1891.
6. Leichner PK. A unified approach to photon and beta particle dosimetry. *J Nucl Med* 1994;35:1721–1729.
7. Giap HB, Macey DJ, Podoloff DA. Development of a SPECT-based treatment planning system for radioimmunotherapy. *J Nucl Med* 1995;36:1885–1894.
8. Hawkins WG, Leichner PK, Yang N-C. The circular harmonic transform for SPECT and boundary conditions on the Fourier transform of the sinogram. *IEEE Trans Med Imaging* 1988;7:135–148.
9. Leichner PK, Hawkins WG, Yang N-C. Quantitative SPECT in radioimmunotherapy [Abstract]. *Antibod Immunoconj Radiopharm* 1990;4:25.
10. Hawkins WG, Yang N-C, Leichner PK. Validation of the CHT algorithm for quantitative SPECT. *J Nucl Med* 1991;32:141–150.
11. Leichner PK, Vriesendorp HM, Hawkins WG, et al. Quantitative SPECT for ^{111}In-labeled antibodies in the livers of beagle dogs. *J Nucl Med* 1991;32:1442–1444.
12. Nelson WR, Hirayama H, Rogers DWO. The EGS4 code system. Stanford Linear Accelerator Center. Report 265; 1985.
13. Bielajew AF, Rogers DWO. PRESTA, the parameter reduced electron-step size transport algorithm for electron Monte Carlo transport. National Research Council of Canada Pub. PIRS-0042; 1991.
14. Burrows TW. The program RADLST. Information Analysis Center Report. Report. BNL-NCS-52142. Brookhaven National Laboratory; Upton, NY: 1988.
15. Proceedings at the 12th annual international conference on the IEEE. *Eng Med Biol Soc* 1990;376–378.
16. Metz CE, Pax X. A unified analysis of exact methods of inventing the two-dimensional exponential radon transform with implications for noise control in SPECT. *IEEE Trans Med Imag* 1995;14:643–658.
17. Hawkins WG, Leichner PK. An intrinsic 3D Wiener filter for the deconvolution of spatially varying collimator blur. *Proceedings of the First IEEE International Conference on Image Processing* 1994;2:163–168.
18. Burrus CS and Parks TW. The discrete Fourier transform. In: Burrus CS, Parks TW, eds. *DFT/FFT and convolution algorithms*, 1st ed. New York: John Wiley & Sons; 1985:21–80.
19. International Commission on Radiation Units and Measurements. *Tissue substitutes in radiation dosimetry and measurement.* ICRU Report 44. Bethesda: Press; ICRU 1988.
20. Cristy M, Eckerman KF. Specific Absorbed Fractions of Energy at Various Ages from Internal Photon Sources. I. Methods. Report ORNL/TM-8381/V1. Oak Ridge, TN: Oak Ridge National Laboratory; 1987.
21. Snyder WS, Ford MR, Warner GG and Watson SB. "S', absorbed dose per unit cumulated activity for selected radionuclides and organs. *MIRD pamphlet no. 11.* New York: Society of Nuclear Medicine; 1975.
22. Sauer OA. Calculation of dose distribution in the vicinity of high-Z interfaces for photon beams. *Med Phys* 1995;22:1685–1690.

Quantitative Blood Flow Measurement of Skeletal Muscle Using Oxygen-15-Water and PET

Ulla Ruotsalainen, Maria Raitakari, Pirjo Nuutila, Vesa Oikonen, Hannu Sipilä, Mika Teräs, M. Juhani Knuuti, Peter M. Bloomfield and Hidehiro Iida

Turku PET Center and Department of Medicine and Nuclear Medicine, University of Turku, Turku, Finland; MRC, Cyclotron Unit, London, United Kingdom; and Department of Radiology and Nuclear Medicine, Research Institute for Brain and Blood Vessels, Akita, Japan

The aim of the present study was to evaluate quantitation of muscle blood flow using [^{15}O]H_2O and PET. **Methods:** The autoradiographic (ARG) and the steady-state methods using PET were used to measure femoral muscle blood flow. A simulation study was performed to examine the errors due to contamination of radioactivity in the blood content in muscle tissue, statistical noise and delay and the dispersion of the input curve in the ARG method. Five separate paired muscle blood flow examinations were carried out for comparison of the ARG and the steady-state techniques, including measurement of muscle blood volume in each subject. To obtain the normal range for resting muscle blood flow, additional measurements with the ARG method were performed in 16 normal subjects. **Results:** When the integration time in ARG was increased to 200–300 sec, the errors due to arterial blood volume, statistical noise, delay and dispersion of the input curve were significantly reduced. Muscle blood flow values in the ARG (200 sec) and the steady-state studies were in good agreement, and each provided an estimated accuracy of 5%. Resting muscle blood flow averaged 3.12 ± 1.55 ml/min · 100 g muscle (range 1.43–6.72 ml/min · 100 g muscle, n = 18). **Conclusion:** The ARG and the steady-state methods provided consistent blood flow values for skeletal muscle when a long tissue integration time (≥200 sec) was applied in the ARG study. Based on the lower effective radiation dose and the shorter total scan duration, the ARG method is favored over the steady-state method in the measurement of muscle blood flow.

Key Words: PET; muscle blood flow; low flow

J Nucl Med 1997; 38:314-319

Measurement of metabolite exchange across skeletal muscle requires quantitation of blood flow through the muscle bed (*1*). Reduced blood flow has been suggested to be one of the mechanisms leading to insulin resistance in skeletal muscle (*2*). Peripheral flow studies have previously been performed with plethysmography (*3*) or dilution techniques (*2,4*), which give a measure of whole limb blood flow, including blood flow to skin, adipose tissue and bone in addition to muscle flow. Direct quantitation of muscle blood flow has been performed using the ^{133}Xe clearance technique (*5,6*), which has techni-

Received Oct. 26, 1995; revision accepted Apr. 3, 1996.

For correspondence or reprints contact: Ulla Ruotsalainen, MSc, Turku PET Center, Kiinamyllynkatu 4–6, FIN-20520 Turku, Finland.